NJC

LETTER

View Article Online
View Journal

Cite this: DOI: 10.1039/c6nj01076h

C–N bond hydrogenolysis of aniline and cyclohexylamine over TaO_x–Al_2O_3†

Mark Bachrach,[ab] Tobin J. Marks*[a] and Justin M. Notestein*[b]

Received (in Nottingham, UK)
7th April 2016,
Accepted 23rd May 2016

DOI: 10.1039/c6nj01076h

www.rsc.org/njc

TaO_x grafted onto Al_2O_3 is investigated for C–N bond cleavage of amines under H_2 pressure. Heteroaromatics such as aniline are stoichiometrically denitrogenated at high temperature, while cyclohexylamine is catalytically denitrogenated. UV-visible and X-ray photoelectron spectroscopy indicate the formation of a stable Ta–N species in the former case.

Highly dispersed, supported Ta complexes have previously been shown to carry out N–H and N–N bond activation under fairly mild conditions. Basset *et al.* have shown that Ta–SiO_2 derived from the organometallic precursor $Ta(CH_2–CMe_3)_3(=CH–CMe_3)$ is able to cleave the N–H bond in NH_3 (108 kcal mol^{-1}) at room temperature[1,2] as well as cleave the N–N triple bond in N_2 (226 kcal mol^{-1}) at 250 °C.[2,3] Here we study related systems for C–N bond cleavage. This reaction is of increasing importance in the hydrotreating process for removing heteroatom impurities (N,O,S) from crude fuels. Hydrodenitrogenation (HDN) is often studied with quinoline as a model reagent since it is representative of a typical impurity within transportation fuel.[4–6] However, there are relatively few studies of HDN over well-defined model catalytic materials.[7,8]

Pd nanoparticles supported on Al_2O_3 are catalysts for quinoline hydrogenation and C–N bond cleavage. We previously reported that adding low levels of Ti-, Ta-, or Mo-oxides to the Al_2O_3 support significantly increases the selectivity to aromatic products (*e.g. n*-propylbenzene instead of *n*-propylcyclohexane).[8] This selectivity change results in a 10–15% reduction in the amount of H_2 required to remove the same number of N atoms. In that report we suggested a mechanism for denitrogenation with the Pd/MO_x materials based on our experiments with downstream intermediates (substituted anilines, cyclohexylamines, benzenes, and cyclohexenes) as well as *in situ* X-ray absorption spectroscopy (XANES/EXAFS). The key step in the denitrogenation process was proposed to be a partial hydrogenation of 2-propylaniline to 1,6-dihydro-2-propylaniline by the Pd nanoparticle, followed by transfer of this reactive intermediate to the metal oxide for deamination. We also showed that the MO_x–Al_2O_3 materials are significantly more active for denitrogenation than bare Al_2O_3.

Here, we further report on the deamination step with TaO_x–Al_2O_3 as a model material in this series. This material is prepared by grafting $Ta(acac)(OEt)_4$ onto Al_2O_3 at a 1.4 wt% Ta loading and calcining the resulting complex in air at 500 °C. This yields an undercoordinated, isolated Ta(v)-oxo species supported on a positively charged Al_2O_3 surface as shown by our previously reported XANES/EXAFS, diffuse reflectance UV-visible spectroscopy (DRUV-vis), and Zeta potential measurements. We now compare the relative activity for C–N bond cleavage in the deamination of cyclohexylamine, aniline, and pentafluoraniline, and postulate a deamination mechanism.

The strength of the C–N bond impacts the minimum temperature at which C–N bond cleavage occurs, the relative propensity for reactant desorption *vs.* conversion, and the ability of the material to turnover catalytically. Here, the material was treated under 10% O_2/Ar for 2 h, followed by pulses of aniline, cyclohexylamine, or pentafluoraniline in hexane at 120 °C under He until the surface is saturated. Temperature programmed reaction (TPRx) under 10% H_2/N_2 is carried out from 150–400 °C (or 500 °C for pentafluoroaniline) (Table 1).

Cleavage of the sp^3C–N bond in cyclohexylamine (87.6 kcal mol^{-1})[2] is relatively facile, and the vast majority (97%, Table 1) of the adsorbed reactant undergoes deamination before it can desorb from the surface. As shown in Fig. 1 (also Table S1, ESI†), a very small percentage of the cyclohexylamine is dehydrogenated to aniline, while C–N bond cleavage gives predominantly cyclohexene (70%) and benzene (29%) with <1% cyclohexane evolving primarily between 250 and 300 °C. The benzene : cyclohexane ratio (36 : 1) approaches the equilibrium ratio (23 : 1),[9]

[a] Department of Chemistry, Northwestern University, 2145 Sheridan Road, Evanston, Illinois 60208, USA. E-mail: t-marks@northwestern.edu
[b] Department of Chemical & Biological Engineering, Northwestern University, 2145 Sheridan Road, Evanston, Illinois 60208, USA. E-mail: j-notestein@northwestern.edu

† Electronic supplementary information (ESI) available. See DOI: 10.1039/c6nj01076h

Table 1 Product distribution from amine desorption and denitrogenation

	150–350 °C		400–500 °C			
T range	Reactant desorption (%)	C–N bond cleavage (%)	Reactant desorption (%)	C–N bond cleavage (%)	mol_{NH_2}/mol_{Ta} [a]	mol_{HC}/mol_{Ta} [b]
C_6H_{11}–NH_2	3.0	96.4	<0.1	0.6	3	110
C_6H_5–NH_2	99.5	0	0.3	0.2	142	0.3
C_6F_5–NH_2	95.4	0	4.6	0	123	0

[a] Total moles reactant desorbed over the entire temperature range, per mol Ta. [b] Total moles C–N bond cleavage products (cyclohexene, cyclohexane, benzene) detected over the entire temperature range, per mol Ta.

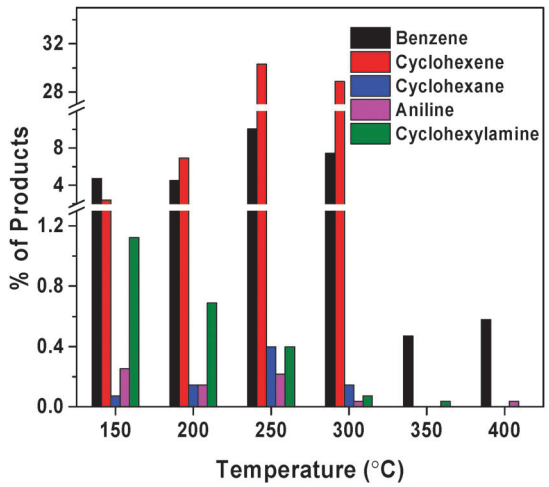

Fig. 1 Temperature programmed reaction of cyclohexylamine over TaO_x–Al_2O_3 from 150–400 °C. The *y*-axis spans three distinct scales.

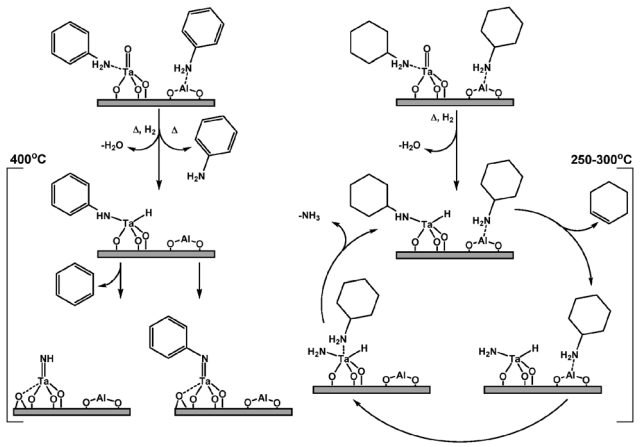

Scheme 1 Proposed steps in the stoichiometric denitrogenation of aniline (left) and catalytic denitrogenation of cyclohexylamine (right). Reactant amines are chemisorbed at the Lewis-acidic, d^0 Ta center and physisorbed on Lewis and Brønsted sites on the residual Al_2O_3 surface. Cyclohexylamine undergoes β-elimination to form a Ta-amido at low temperatures and is displaced by other adsorbed cyclohexylamine substrate molecules that migrate from the Al_2O_3 surface. Aniline denitrogenates *via* direct sp^2C–N bond cleavage to give an unreactive Ta-imido; this occurs at temperatures above which most of the aniline has desorbed.

however the cyclohexene produced exceeds the expected equilibrium amount by orders of magnitude. This product distribution suggests that cyclohexylamine undergoes β-elimination to cyclohexene as the primary product (Scheme 1), which then slowly approaches the benzene/ cyclohexene/ cyclohexane equilibrium. Direct C–N bond hydrogenolysis is inconsistent with the high cyclohexene selectivity. In contrast, cyclohexylamine denitrogenation is catalytic, with 110 molecules of product detected per Ta atom (Table 1), consistent with a mechanism where amines adsorbed on the bare alumina surface readily diffuse to the Ta sites where they undergo deamination.

In contrast to cyclohexylamine, aniline C–N bond cleavage involves a significantly stronger sp^2C–N bond (102.6 kcal mol^{-1}).[2] Substoichiometric formation of exclusively benzene (0.3 per Ta, Table 1) is detected at 400 °C, but the vast majority of the aniline is desorbed intact as a broad feature at lower temperatures (Fig. S1, ESI†). Even at 400 °C, where >99% of the aniline had previously desorbed, more aniline desorbs intact than is denitrogenated, indicating that the surface species formed from aniline denitrogenation is chemically inert even at these conditions. Similarly, we previously observed catalytic denitrogenation of methylcyclohexylamine but only stoichiometric denitrogenation of 2-propylaniline over TaO_x–Al_2O_3 under high H_2 pressures in a batch reactor.[8] The lack of catalytic turnover even in the presence of excess reactant requires the formation of an inert surface species as a co-product of aniline denitrogenation.

The electron-withdrawing aromatic ring of pentafluoroaniline and the geometric influence of the C–F groups further shorten and strengthen the C–N bond.[10] As expected then, this molecule undergoes only intact desorption, with no C–N bond cleavage products detected up to 500 °C.

Unreactive Ta-imido species were observed as products by Basset *et al.* in NH_3 or N_2 cleavage by supported Ta,[1,3] and we propose (Scheme 1) to form similar Ta-imido and Ta-arylimido species during aniline denitrogenation. The used material from aniline TPRx to 400 °C was subsequently studied by DRUV-vis spectroscopy, X-ray photoelectron spectroscopy, and temperature programmed reduction with H_2 to provide evidence for such a species.

A Tauc plot of the direct band gap derived from the DRUV-vis spectra (Fig. 2) shows that the used TaO_x–Al_2O_3 material has three optical edges at 4.7 eV, 3.9 eV and 3.8 eV. All three edges are significantly lower than those of the freshly calcined material (5.4 eV). Al_2O_3 is optically transparent to much higher energies (bandgap = 8.8 eV).[11] Bulk Ta_2O_5 has a bandgap of 4.1 eV which is approximately the correct energy,[12] but prior XANES/EXAFS showed no change in Ta coordination number indicative of the

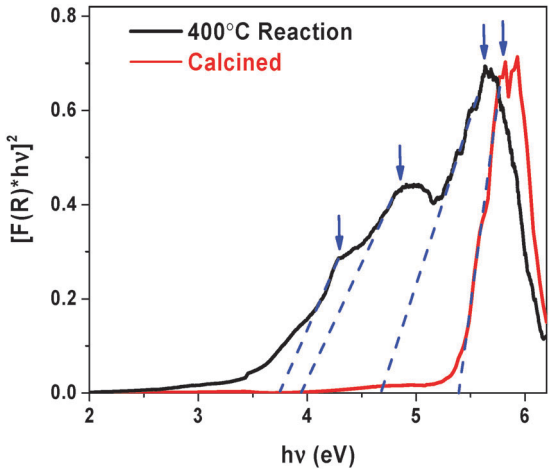

Fig. 2 Tauc plot for the direct band gap of TaO_x–Al_2O_3 materials after calcination and aniline TPRx to 400 °C. Optical edges at 5.4 eV (calcined) and 4.7 eV (after 400 °C reaction) correspond to alumina oxygen-to-Ta transitions, while optical edges at 3.9 eV and 3.8 eV correspond to LMCT transitions from the imido.

aggregation of the TaO_x domains.[8] Bulk Ta_3N_5 has a much lower bandgap (2.1 eV) than bulk Ta_2O_5[12] supporting the hypothesis that the shift in bandgap from the higher bandgap in the freshly calcined material to the lower bandgap in the used material indicates the transformation of isolated Ta–oxo to isolated Ta-imido sites. In contrast to these bulk materials, which do not appear to be a good spectroscopic fit for the formed structures, Wolczanski *et al.* reported a (silox)Ta═NPh complex whose geometry is very similar to that drawn in Scheme 1 and which has very similar optical features.[13] This complex was shown to have two primary features at 246 nm (peak maximum at 5.0 eV) and 285 nm (peak maximum at 4.4 eV), very similar to the features in Fig. 3 with peak maxima at 4.9 eV (edge at 3.9 eV) and 4.3 eV (edge at 3.8 eV). The complex also shows a high energy feature at 215 nm (peak maximum at 5.8 eV) from the siloxide ligand, similar to the indicated feature with a peak maximum at 5.7 eV (edge at 4.7 eV). We thus assign the high energy feature in the experimental spectrum (edge at 4.7 eV) to an LMCT from alumina oxygens to an isolated Ta═NH or Ta═NPh center, which is shifted to lower energy than the analogous interactions with a Ta═O center (edge at 5.4 eV) in the freshly calcined material, due to the significantly more electron-donating character of the imido or arylimido group.

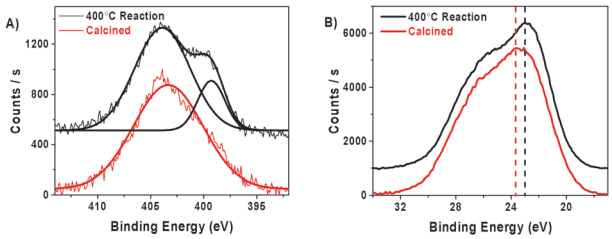

Fig. 3 Fitted XPS spectra of TaO_x–Al_2O_3 after calcination and aniline TPRx to 400 °C. (A) N 1s orbital (399 eV) and Ta $4p_{3/2}$ orbital (404 eV) and (B) Ta 4f orbital.

The lower energy transitions (edges below 4.0 eV) are then assigned as ligand-to-metal charge transfer bands (LMCT) from the imido or arylimido itself, as reported by Wolczanski *et al.*

Comparison of the XPS spectra of the freshly calcined TaO_x–Al_2O_3 material with the material from the aniline TPRx to 400 °C shows the appearance of a N 1s peak at 399 eV on the shoulder of the Ta $4p_{3/2}$ orbital peak at 404 eV (Fig. 3A). The Ta $4f_{5/2}$ peak is also slightly redshifted (Fig. 3B) due to less energetically demanding electron ejection in Ta═NR (23.0 eV) than in Ta═O (23.5 eV).[14,15]

Temperature programmed reduction (TPR) in H_2 was also carried out with the freshly calcined and used materials (Fig. 4). Both traces show three broad reduction events. For the calcined catalyst, the first reduction has an onset temperature of ~200 °C and a maximum near 300 °C, corresponding to peak activity in cyclohexylamine denitrogenation. In earlier studies,[8] no reduction of the Ta oxidation state was observed at 275 °C in H_2, so this first feature that begins near 200 °C is assigned to addition of H_2 across the Ta═O bond. Likewise, a second feature with an onset of ~500 °C corresponds to a similar amount of H_2 consumption, and is assigned to hydrogenolysis of the Ta–OH bond, giving a Ta hydride. Finally, the Ta atoms are reduced to Ta nanoparticles or isolated Ta(III) sites above ~670 °C.

For the used catalyst, there is a significant shift in the temperature of the first reduction event, largely because the material has already seen reducing conditions up to 400 °C. The onset of H_2 uptake is at ~450 °C, with a maximum of ~530 °C. By analogy to above, this feature is assigned as reduction of Ta═NH and Ta═NPh groups on the surface. The increase in temperature necessary for H_2 addition across the Ta-imido relative to the Ta–oxo is attributed to the markedly higher Ta-imido bond order compared to that of a Ta–oxo bond.[16,17] A second feature immediately follows, which we assign to hydrogenolysis of the remaining Ta–NHR bonds (amines and amidos). Finally, reduction of Ta again has an onset of ~680 °C. As expected from stoichiometry, all features are similar in area.

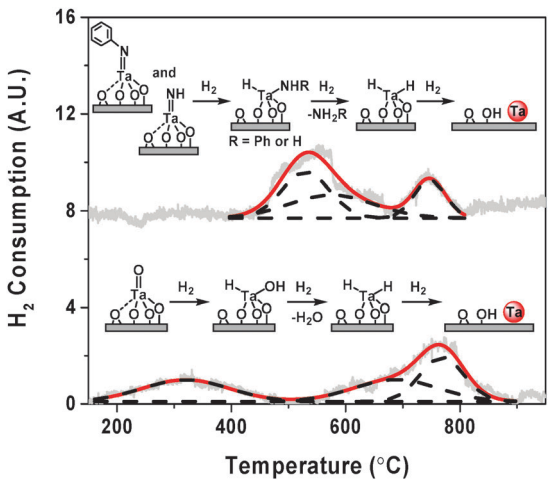

Fig. 4 Temperature programmed reduction in H_2 of the calcined material TaO_x–Al_2O_3 (bottom) and the material after aniline TPRx to 400 °C (top). Note that after 800 °C, the *x*-axis corresponds to a 3 h isothermal hold.

Overall, these results illustrate how the dispersed metal oxide sites contribute to the cleavage of C–N bonds under hydrogenolysis conditions. These results require that the direct cleavage of the sp^2C–N bond in aniline proceeds *via* a different mechanism than that of the sp^3C–N bond in cyclohexylamine. Finally, this conclusion indicates that reactivity enhancements in quinoline hydrodenitrogenation over Pd/TaO_x–Al_2O_3 below 400 °C are consistent with our previously-proposed mechanism of partial ring hydrogenation over Pd, followed by deamination assisted by the Ta sites, rather than direct sp^2C–N bond cleavage.

Experimental

Material synthesis

TaO_x–Al_2O_3 was synthesized by our previously published method.[8] Briefly, Ta(acac)$(OEt)_4$ was grafted onto Al_2O_3 in toluene (Selecto Al_2O_3 A; 165 $m^2\ g^{-1}$) at a 1.4 wt% metal loading to form Ta(acac)$(OEt)_2$–Al_2O_3. The material was then calcined for 6 h in air at 500 °C in a muffle furnace to form the TaO_x–Al_2O_3 species prior to loading in the reactor.

Hydrodenitrogenation

TaO_x–Al_2O_3 (300 mg) was loaded into a quartz u-tube reactor in an Altamira AMI-200 reactor system. The material was calcined at 500 °C under 25 sccm 10% O_2/Ar for 2 h. 300 μL reactant (cyclohexylamine, aniline, or pentafluoraniline) was then slowly injected over an hour under He at 120 °C. The pentafluoroaniline was diluted in hexanes for injection since it is a solid at room temperature. The reactor was then purged with He at 120 °C for an additional 2 h to allow for loosely physisorbed reactant to be removed from the material. The reactor was then heated in 10% H_2/N_2 at 30 sccm by stepwise ramps at 5 °C min^{-1} and then 3 h holds at 150, 200, 250, 300, 350, and 400 °C for the aniline and cyclohexylamine reactions, and 450 °C and 500 °C for the pentafluoroaniline reaction. All products were quantified with a Pfeiffer process mass spectrometer. *m*/*z* assignments: cyclohexylamine = 99, aniline = 93, pentafluoraniline = 183, pentafluorocyclohexylamine = 189, cyclohexene = 82, benzene = 78, cyclohexane = 84, pentafluorocyclohexene = 172, pentafluorocyclohexane = 174, pentafluorobenzene = 168.

Materials characterization

Temperature programmed reduction used 1.00 g material in an Altamira AMI-200 with a TCD detector. Reductions were run with a 3 °C min^{-1} ramp under 10% H_2/N_2 until 800 °C and then held at 800 °C for 3 h. An acetone/dry ice bath trapped H_2O, NH_3, and other condensables to ensure that the TCD only measured H_2 consumption. Data were analyzed in OriginLab 9.1. XPS was performed on a Thermo Scientific ESCALAB 250XI with Al K-alpha radiation with a flood gun. Samples were referenced to carbon with a binding energy of 284.8 eV. Samples were fitted to a Gaussian in OriginLab 9.1. UV-visible spectra from 800–200 nm were collected on a Shimadzu 3600 equipped with a Harrick Praying Mantis Diffuse Reflectance accessory. Kubelka Munk pseudoabsorbances were calculated relative to PTFE as a perfect reflector. Optical edges were calculated based on the intercept of the tangent line in a plot of $[F(R) \times h\nu]^2$ *vs.* $h\nu$.

Acknowledgements

The authors acknowledge the ACS Petroleum Research Fund and the DOE Office of Basic Sciences Grants SC-0006718 (MB, JMN) and 86ER1311 (MB, TJM) for funding. The authors also acknowledge N. M. Schweitzer and L. M. Savereide for technical assistance. This work made use of the Keck-II facility (NUANCE Center – Northwestern University), which has received support from the W. M. Keck Foundation, Northwestern's Institute for Nanotechnology's NSF-sponsored Nanoscale Science & Engineering Center (EEC-0118025/003), both programs of the National Science Foundation; the State of Illinois; and Northwestern University. The CleanCat Core facility acknowledges funding from the Department of Energy DE-FG02-03ER15457 used for the purchase of the Altamira AMI-200.

Notes and references

1 P. Avenier, A. Lesage, M. Taoufik, A. Baudouin, A. De Mallmann, S. Fiddy, M. Vautier, L. Veyre, J. M. Basset, L. Emsley and E. A. Quadrelli, *J. Am. Chem. Soc.*, 2007, **129**, 176–186.
2 Y.-R. Luo, *Comprehensive Handbook of Chemical Bond Energies*, CRC Press, Boca Raton, 2007.
3 P. Avenier, M. Taoufik, A. Lesage, X. Solans-Monfort, A. Baudouin, A. De Mallmann, L. Veyre, J. M. Basset, O. Eisenstein, L. Emsley and E. A. Quadrelli, *Science*, 2007, **317**, 1056–1060.
4 M. J. Girgis and B. C. Gates, *Ind. Eng. Chem. Res.*, 1991, **30**, 2021–2058.
5 M. Jian and R. Prins, *J. Catal.*, 1998, **179**, 18–27.
6 J. C. Schlatter, S. T. Oyama, J. E. Metcalfe and J. M. Lambert, *Ind. Eng. Chem. Res.*, 1988, **27**, 1648–1653.
7 M. Bachrach, T. J. Marks and J. M. Notestein, *ACS Catal.*, 2016, **6**, 1455–1476.
8 M. Bachrach, N. Morlanes-Sanchez, C. P. Canlas, J. T. Miller, T. J. Marks and J. M. Notestein, *Catal. Lett.*, 2014, **144**, 1832–1838.
9 G. G. Janz, *J. Chem. Phys.*, 1954, **22**, 751.
10 P. Wojciechowski, *J. Fluorine Chem.*, 2013, **154**, 7–15.
11 R. H. French, *J. Am. Ceram. Soc.*, 1990, **73**, 477–489.
12 M. Harb, P. Sautet, E. Nurlaela, P. Raybaud, L. Cavallo, K. Domen, J. M. Basset and K. Takanabe, *Phys. Chem. Chem. Phys.*, 2014, **16**, 20548–20560.
13 E. B. Hulley, J. B. Bonanno, P. T. Wolczanski, T. R. Cundari and E. B. Lobkovsky, *Inorg. Chem.*, 2010, **49**, 8524–8544.
14 Q. S. Gao, S. N. Wang, Y. C. Ma, Y. Tang, C. Giordano and M. Antonietti, *Angew. Chem., Int. Ed.*, 2012, **51**, 961–965.
15 W. J. Chun, A. Ishikawa, H. Fujisawa, T. Takata, J. N. Kondo, M. Hara, M. Kawai, Y. Matsumoto and K. Domen, *J. Phys. Chem. B*, 2003, **107**, 1798–1803.
16 T. R. Cundari, *Chem. Rev.*, 2000, **100**, 807–818.
17 T. I. Gountchev and T. D. Tilley, *J. Am. Chem. Soc.*, 1997, **119**, 12831–12841.

